Symmetries of Shamrocks II: Axial Shamrocks

Mihai Ciucu*
Department of Mathematics
Indiana University
Bloomington, Indiana 47405. U.S.A.
mciucu@indiana.edu

Submitted: Oct 24, 2017; Accepted: Apr 9, 2018; Published: Jun 8, 2018

Abstract

The first paper in this series presented the enumeration of cyclically symmetric, and cyclically symmetric and transpose complementary lozenge tilings of a hexagon with a shamrock removed from its center. In this article we address the transpose complementary case. The results we prove are in fact more general and allow us to give an extension of the symmetric case of the original hexagonal regions with shamrocks removed from their center, to what we call axial shamrocks. For the latter, the transpose complementary case is the only symmetry class besides the one requiring no symmetries. The enumeration of both of these follows from our results.

Mathematics Subject Classifications: 05A15, 05A17

1 Introduction: Axial shamrocks

Inspired by the beauty of MacMahon's formula [18] stating that the number of lozenge tilings of a hexagonal region of side-lengths x, y, z, x, y, z (in cyclic order) on a triangular lattice is

$$\prod_{i=1}^{x}\prod_{j=1}^{y}\prod_{k=1}^{z}\frac{i+j+k-1}{i+j+k-2},$$

and driven by the desire to generalize it, in [8] we considered hexagons on the triangular lattice with shamrock-shaped regions (consisting of a central triangle with three additional triangular lobes attached to its vertices) removed from their center, and proved product formulas giving the number of their lozenge tilings. Motivated by the celebrated study

*Research supported in part by NSF grant DMS-1101670 and DMS-1501052.

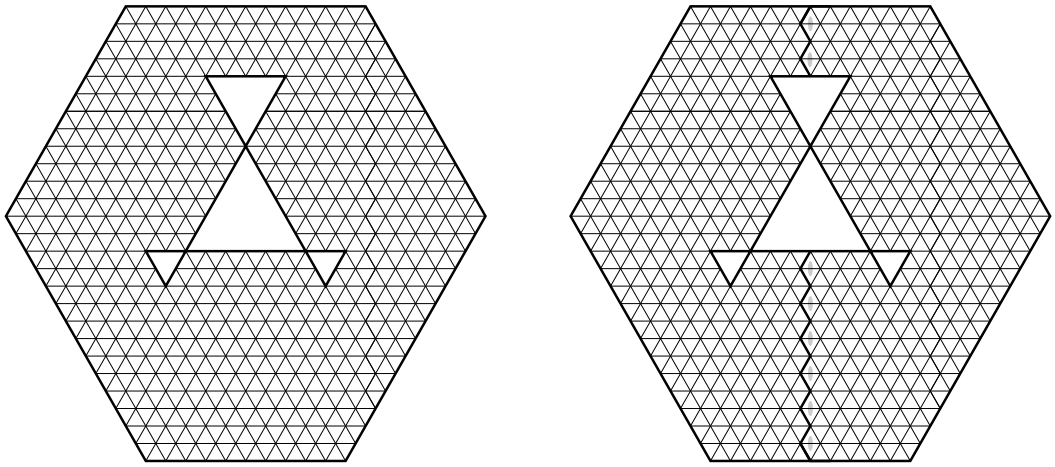

Figure 1: An axial shamrock (left); regions obtained by factorization theorem (right).

of symmetry classes of plane partitions (see [1][20][17][21][14] and the survey [2] for more recent developments), we took up the problem of enumerating their symmetry classes in [12], where we solved two of the six new counting problems arising this way. In this paper we solve a third symmetry class, the one corresponding to transpose complementary plane partitions. We use Kuo's graphical condensation method (see [15] and [16]) to prove our results. In order for this method to work, we have to extend the family of regions we consider, and we end up solving the more general case of axial shamrock regions, defined below.

Consider an arbitrary vertically-symmetric hexagon on the triangular lattice, and remove from it a shamrock-shaped region that is also vertically symmetric about the same symmetry axis as the hexagon, in such a way that the remaining region has the same number of up- and down-pointing unit triangles. We call the resulting region an *axial shamrock* (see the picture on the left in Figure 1 for an example). Note that in an axial shamrock the removed shamrock-shaped core — which we will often call simply the *core* — can be freely translated up and down the symmetry axis; for precisely one position among these is the resulting region an S-cored hexagon as defined in [8].

Axial shamrocks have just one symmetry class besides the case of requiring no symmetry, corresponding to its tilings being vertically symmetric. The transpose complementary case of the original S-cored hexagons considered in [8] and [12] follows as a special case of this, as we explain in the next section.

In Section 2 we present the statements of our main results. In order to prove them, we first need to enumerate the tilings of two specific families of regions, which we address in Sections 3 and 4. We prove our main results in Section 5. Section 6 poses an asymptotics problem and presents some interesting data. In Section 7 we present some concluding remarks.

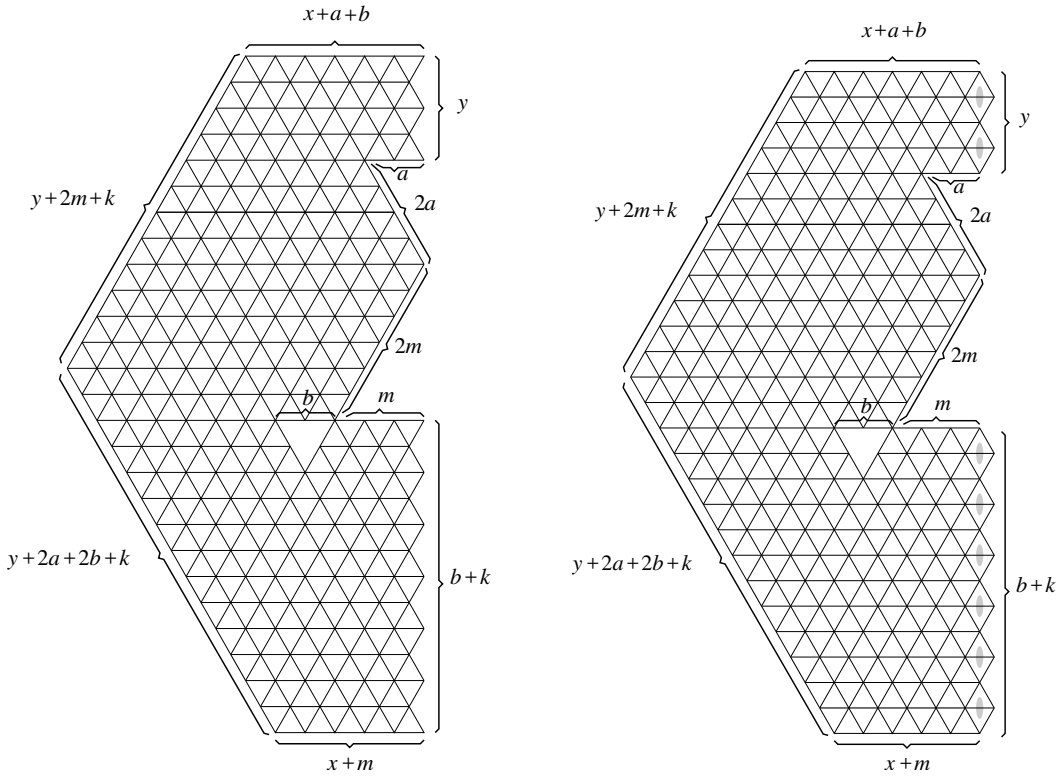

Figure 2: The regions $R_{x,y,k}(m,a,b)$ (left) and $R'_{x,y,k}(m,a,b)$ (right) for $x=2$, $y=2$, $k=4$, $m=3$, $a=2$, $b=2$.

2 Statement of main results

Assuming that the top and bottom sides of the outer hexagon, as well as the sides of the central and top lobe of the shamrock core have even length, the two "halves" obtained by applying the factorization theorem of [3] to the axial shamrock are as shown on the right in Figure 1. This leads us to consider the following two families of regions.

Let x, y, k, m, a and b be non-negative integers. We define $R_{x,y,k}(m,a,b)$ to be the region described on the left in Figure 2: $x+m$, m, a and b are the lengths of the indicated segments, while y and k are the number of "bumps" (zig-zags) in the indicated portions of the boundary.

The region $R'_{x,y,k}(m,a,b)$ is defined analogously, using the picture on the right in Figure 2. The shaded ovals indicate, throughout this paper, that the corresponding lozenge positions are weighted by $1/2$.

For both the R- and the R'-regions, the chosen parametrization ensures that the half-shamrock core is inside (or possibly touches the outer boundary of) the half-hexagon.

The main results of this paper are the enumeration of lozenge tilings of these regions, presented in Theorems 1 and 2 below. They allow us to deduce the symmetry classes of axial shamrocks (see Corollaries 3 and 4).

The formulas we obtain involve the following expressions, known from previous results in the literature, for the enumeration of lozenge tilings of hexagonal regions with a maxi-

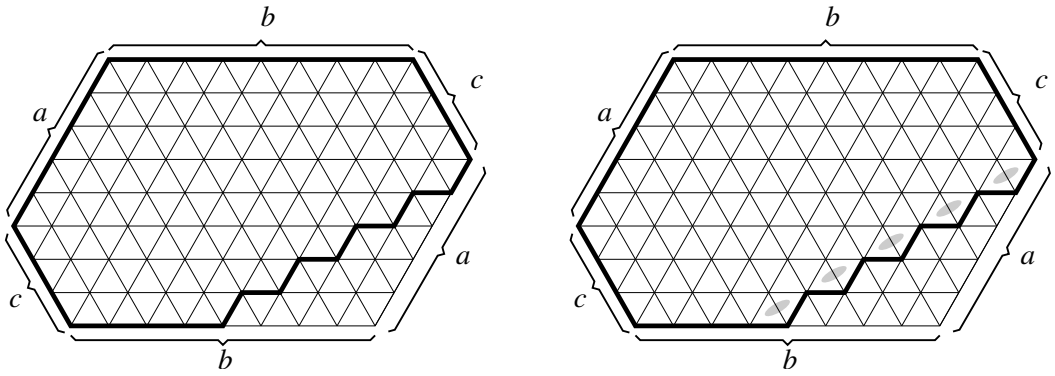

Figure 3: The regions $H_s(a,b,c)$ (left) and $H'_s(a,b,c)$ (right) for $a=5$, $b=8$, $c=3$.

mal staircase shape removed from one of their corners.

For non-negative integers a, b and c, define $H_s(a,b,c)$ to be the region obtained from the hexagon of side-lengths a, b, c, a, b, c (in cyclic order, starting with the northwestern side) by removing the maximal staircase shape that fits in its southeastern corner (see the picture on the left in Figure 3 for an illustration). Let $H'_s(a,b,c)$ be the region obtained from $H_s(a,b,c)$ by weighting the lozenge positions that fit in the folds of its southeastern boundary by 1/2 (this is illustrated on the right in Figure 3). For non-negative integers a, b and c with $a \leqslant b+1$, set[1]

$$P(a,b,c) := \prod_{i=1}^{a} \prod_{j=1}^{b-a+1} \frac{c+i+j-1}{i+j-1} \prod_{j=b-a+2}^{b-a+i} \frac{2c+i+j-1}{i+j-1}. \tag{1}$$

and for non-negative integers a, b and c with $a \leqslant b$, set

$$P'(a,b,c) := \frac{1}{2^a} \prod_{i=1}^{a} \prod_{j=1}^{b-a} \frac{c+i+j-1}{i+j-1} \prod_{j=b-a+i}^{b} \frac{2c+i+j-1}{i+j-1}. \tag{2}$$

The lozenge tilings of the regions $H_s(a,b,c)$ were enumerated by Proctor [19], who proved that[2], for $a \leqslant b$,

$$\mathrm{M}(H_s(a,b,c)) = P(a,b,c). \tag{3}$$

One readily sees that (3) holds also for $a = b+1$ (upon removing forced lozenges, the case $a = b+1$ reduces to the case $a = b$).

[1] Under the indicated restrictions for the integers a, b and c, it is possible for some of the product limits involved in (1) and (2) to be out of order — more precisely, for the upper limit to be one unit less than the lower limit. In all such instances the corresponding product is taken to be 1.

[2] Throughout the paper, $\mathrm{M}(G)$ stands for the number of perfect matchings of the graph G, or, in case the edges of G carry weights, it denotes the sum over all perfect matchings μ of G of the weight of μ (the latter being the product of the weights of the edges that make up μ). Since lozenge tilings of a region R can be identified with perfect matchings of the planar dual graph of R, we also use $\mathrm{M}(R)$ to denote the (possibly weighted) count of lozenge tilings of the region R (in this paper, the only tiling weights that occur are 1 and 1/2; the latter appear precisely when a lozenge occupies a tile position weighted by 1/2; all these locations are indicated in the figures by shaded ovals).

The lozenge tilings of the regions $H'_s(a,b,c)$ were enumerated by Ciucu and Krattenthaler [4], who showed that for $a \leqslant b$

$$\mathrm{M}(H'_s(a,b,c)) = P'(a,b,c). \tag{4}$$

The formulas we present for the enumeration of the tilings of the regions of type R and R' defined above involve Pochhammer symbols that may have negative index. Recall that, for any integer k (positive or negative) the Pochhammer symbol $(x)_k$ is defined as

$$(a)_k = \begin{cases} a(a+1)\cdots(a+k-1), & k \geqslant 0 \\ \dfrac{1}{(a-1)(a-2)\cdots(a-k)}, & k < 0 \end{cases} \tag{5}$$

All the Pochhammer symbols that occur in this paper are to be understood as being defined by this formula.

The main results of this paper are the following.

Theorem 1. *For any non-negative integer values of the parameters x, y, k, m, a, b, the number of lozenge tilings of the region $R_{x,y,k}(m,a,b)$ is given by*

$$\begin{aligned}
\mathrm{M}(R_{x,y,k}(m,a,b)) &= \frac{P(y+2a+2b+k-1, y+2a+2b+k-1, x+m)}{P(y+2a+2b+k-1, y+2a+2b+k-1, m)} \\
&\times P(k+b-1, k+b-1, m) P(y+2a, y+2a+2m-1, b) P(y-1, y-1, a) \\
&\times \prod_{i=1}^{a} \frac{\left(m+i+\frac{1}{2}\right)_{y+2a-2i} (m+i)_{y+2a-2i+1}}{\left(b+m+i+\frac{1}{2}\right)_{y+2a-2i} (b+m+i)_{y+2a-2i+1}} \\
&\times \prod_{i=1}^{m} \frac{(x+m-i+1)_{y+2a+b} (x+m+i+k+b)_{y+2a+b}}{(m-i+1)_{y+2a+b} (m+i+k+b)_{y+2a+b}} \\
&\times \prod_{i=1}^{a} \frac{(m+i+k+b)_{y+2a-k-2i+1} \left(m+i+\frac{1}{2}\right)_{y+2a+2b+k-2i}}{(x+m+i+k+b)_{y+2a-k-2i+1} \left(x+m+i+\frac{1}{2}\right)_{y+2a+2b+k-2i}} \\
&\times \prod_{i=1}^{b} \frac{(k+b-i+1)_{y+2m+2a-k+2i-1} \left(m+a+i+\frac{1}{2}\right)_{y+2b+k-2i}}{(x+k+b-i+1)_{y+2m+2a-k+2i-1} \left(x+m+a+i+\frac{1}{2}\right)_{y+2b+k-2i}},
\end{aligned} \tag{6}$$

where $P(a,b,c)$ is given by (1) when its arguments are non-negative, and is defined to equal 1 otherwise.

Theorem 2. *For any non-negative integer values of the parameters x, y, k, m, a, b, the number of lozenge tilings of the region $R'_{x,y,k}(m,a,b)$ is given by*

$$\begin{aligned}
\mathrm{M}(R'_{x,y,k}(m,a,b)) &= 2^{y+2a}\frac{P'(y+2a+2b+k,y+2a+2b+k,x+m)}{P'(y+2a+2b+k,y+2a+2b+k,m)}\\
&\times P'(k+b,k+b,m)P'(y+2a,y+2a+2m,b)P'(y,y,a)\\
&\times\prod_{i=1}^{a}\frac{(m+i)_{y+2a-2i+1}\left(m+i-\frac{1}{2}\right)_{y+2a-2i+2}}{(b+m+i)_{y+2a-2i+1}\left(b+m+i-\frac{1}{2}\right)_{y+2a-2i+2}}\\
&\times\prod_{i=1}^{m}\frac{(x+m-i+1)_{y+2a+b}(x+m+i+k+b)_{y+2a+b}}{(m-i+1)_{y+2a+b}(m+i+k+b)_{y+2a+b}}\\
&\times\prod_{i=1}^{a}\frac{(m+i+k+b)_{y+2a-k-2i+1}\left(m+i-\frac{1}{2}\right)_{y+2a+2b+k-2i+2}}{(x+m+i+k+b)_{y+2a-k-2i+1}\left(x+m+i-\frac{1}{2}\right)_{y+2a+2b+k-2i+2}}\\
&\times\prod_{i=1}^{b}\frac{(k+b-i+1)_{y+2m+2a-k+2i-1}\left(m+a+i-\frac{1}{2}\right)_{y+2b+k-2i+2}}{(x+k+b-i+1)_{y+2m+2a-k+2i-1}\left(x+m+a+i-\frac{1}{2}\right)_{y+2b+k-2i+2}},
\end{aligned}\tag{7}$$

where $P'(a,b,c)$ *is given by* (2).

We can now present the formulas that give the enumeration of the symmetry classes of axial shamrocks.

For non-negative integers x, y, k, m, a and b, define the axial shamrock $AS_{x,y,k}(m,a,b)$ to be the region obtained from the hexagon of side lengths $2x+2a+2b$, $y+2m+k$, $y+2a+2b+k$, $2x+2m$, $y+2a+2b+k$, $y+2m+k$ (clockwise from top) by removing from it the shamrock-shaped core indicated in Figure 4, placed symmetrically with respect to the vertical symmetry axis of the hexagon. This definition assumes that the central and top lobes of the core have even side-lengths, and that the top and bottom sides of the outer boundary are also even. For the remaining cases there exist enumeration formulas very similar to the ones we present below, but since it captures all the features of the general case, in the interest of clarity we present the formulas just for the case introduced above.

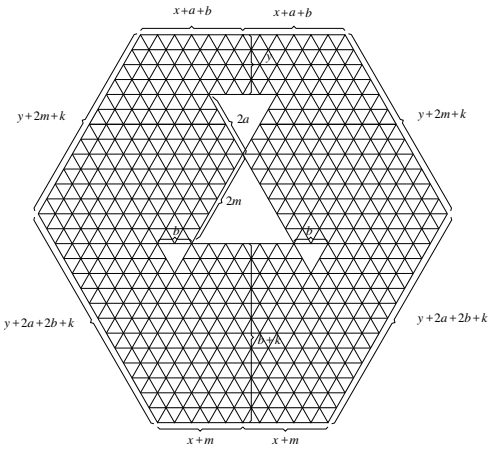

Figure 4: The axial shamrock $AS_{x,y,k}(m,a,b)$ for $x=5$, $y=2$, $k=4$, $m=3$, $a=2$, $b=2$.

Corollary 3. *For all non-negative integers x, y, k, m, a and b, the number of lozenge tilings of the axial shamrock $AS_{x,y,k}(m,a,b)$ is given by*

$$\mathrm{M}(AS_{x,y,k}(m,a,b)) = 2^{y+k+b}\mathrm{M}(R_{x,y,k}(m,a,b))\mathrm{M}(R'_{x,y,k}(m,a,b)),$$

where the quantities on the right hand side above are given by the formulas of Theorems 1 and 2.

Proof. The statement follows by applying the factorization theorem of [3] to the axial shamrock $AS_{x,y,k}(m,a,b)$, and using Theorems 1 and 2. □

Corollary 4. *For all non-negative integers x, y, k, m, a and b, the number of vertically symmetric lozenge tilings of the axial shamrock $AS_{x,y,k}(m,a,b)$ is equal to*

$$\mathrm{M}_{|}(AS_{x,y,k}(m,a,b)) = \mathrm{M}(R_{x,y,k}(m,a,b)),$$

where the quantity on the right hand side above is given by the formula of Theorem 1.

Proof. This follows directly from Theorem 1 and the fact that the vertically symmetric lozenge tilings of the axial shamrock $AS_{x,y,k}(m,a,b)$ are in one-to-one correspondence with the tilings of the region $R_{x,y,k}(m,a,b)$. □

Remark 1. The motivating case of the S-cored hexagons of [8] clearly follows as a special case of Corollary 4.

Our proofs are based on Kuo's graphical condensation method [15]. For convenience, we include below the two forms of it that we will employ.

Theorem 5. *[15, Kuo] Let $G = (V_1, V_2, E)$ be a plane bipartite graph in which $|V_1| = |V_2|$. Let vertices α, β, γ and δ appear cyclically on a face of G. If $\alpha, \gamma \in V_1$ and $\beta, \delta \in V_2$, then*

$$\begin{aligned}\mathrm{M}(G)\mathrm{M}(G-\{\alpha,\beta,\gamma,\delta\}) =& \mathrm{M}(G-\{\alpha,\beta\})\mathrm{M}(G-\{\gamma,\delta\})\\ &+\mathrm{M}(G-\{\alpha,\delta\})\mathrm{M}(G-\{\beta,\gamma\}).\end{aligned} \tag{8}$$

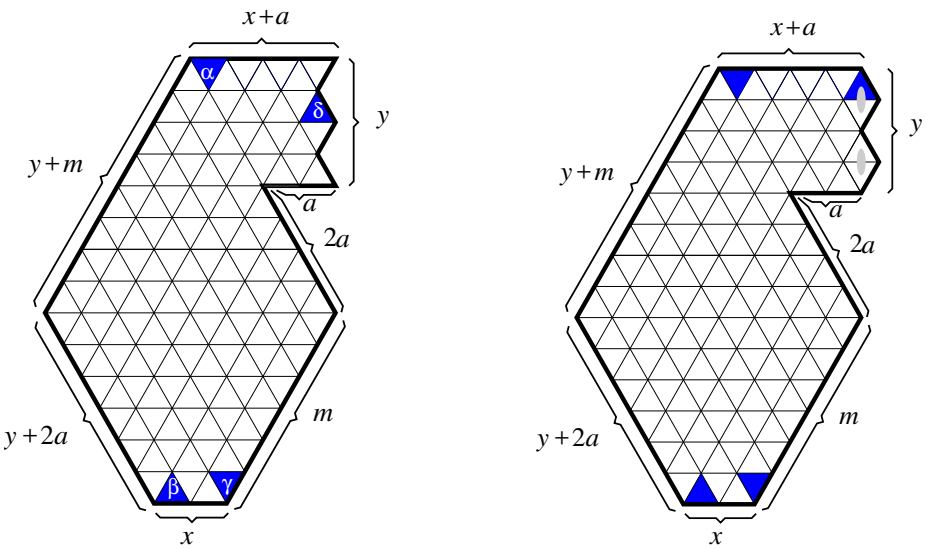

Figure 5: Applying Kuo condensation for periscope regions.

Theorem 6. *[15, Kuo] Let $G = (V_1, V_2, E)$ be a plane bipartite graph in which $|V_1| = |V_2| + 1$. Let vertices α, β, γ and δ appear cyclically on a face of G. If $\alpha, \beta, \gamma \in V_1$ and $\delta \in V_2$, then*

$$\begin{aligned}\mathrm{M}(G-\beta)\mathrm{M}(G-\{\alpha,\gamma,\delta\}) =& \mathrm{M}(G-\alpha)\mathrm{M}(G-\{\beta,\gamma,\delta\}) \\ &+\mathrm{M}(G-\gamma)\mathrm{M}(G-\{\alpha,\beta,\delta\}).\end{aligned} \tag{9}$$

3 Periscope regions Γ and Γ'

For any non-negative integers x, y, m, a, define the periscope region $\Gamma_{x,y}(m,a)$ to be the region described in the picture on the left in Figure 5. The periscope region $\Gamma'_{x,y}(m,a)$ is obtained from it by augmenting it with y unit rhombi that fit in the folds of the top part of its right boundary, as illustrated in the picture on the right in Figure 5 (the shaded ovals indicate lozenge positions weighted by $1/2$).

The purpose of this section is to provide enumeration formulas for the lozenge tilings of the regions $\Gamma_{x,y}(m,a)$ and $\Gamma'_{x,y}(m,a)$.

Theorem 7. *For any non-negative integers x, y, m and a, the number of lozenge tilings of the periscope region $\Gamma_{x,y}(m,a)$ is given by*

$$\begin{aligned}\mathrm{M}(\Gamma_{x,y}(m,a)) = & P(y-1,y-1,a)P(y+2a,y+2a+m-1,x) \\ & \times \prod_{i=1}^{a} \frac{\left(\frac{m}{2}+i+\frac{1}{2}\right)_{y+2a-2i}\left(\frac{m}{2}+i\right)_{y+2a-2i+1}}{\left(x+\frac{m}{2}+i+\frac{1}{2}\right)_{y+2a-2i}\left(x+\frac{m}{2}+i\right)_{y+2a-2i+1}},\end{aligned} \tag{10}$$

where $P(a,b,c)$ is given by (1) *when all its arguments are non-negative, and is equal to* 1 *otherwise.*

Proof. Apply the version of Kuo condensation stated in Theorem 5, with monomers $\alpha, \beta, \gamma, \delta$ chosen as indicated[3] on the left in Figure 5. We obtain (see Figure 6)

$$\begin{aligned}\mathrm{M}(\Gamma_{x,y}(m,a))\mathrm{M}(\Gamma_{x,y-1}(m-1,a)) = & \\ & \mathrm{M}(\Gamma_{x-1,y}(m-1,a))\mathrm{M}(\Gamma_{x+1,y-1}(m-1,a)) \\ & + \mathrm{M}(\Gamma_{x,y-1}(m,a))\mathrm{M}(\Gamma_{x,y}(m-1,a)),\end{aligned} \tag{11}$$

for all integers $x, y, m \geqslant 1$ and $a \geqslant 0$ (so that all the involved regions are defined).

[3] More precisely, we view the region $\Gamma_{x,y}(m,a)$ as a planar graph whose vertices are the unit triangles inside it, and whose edges connect two vertices precisely if the corresponding unit triangles share an edge. Then we apply Theorem 5 to this graph, with vertices $\alpha, \beta, \gamma, \delta$ corresponding to the indicated four unit triangles.

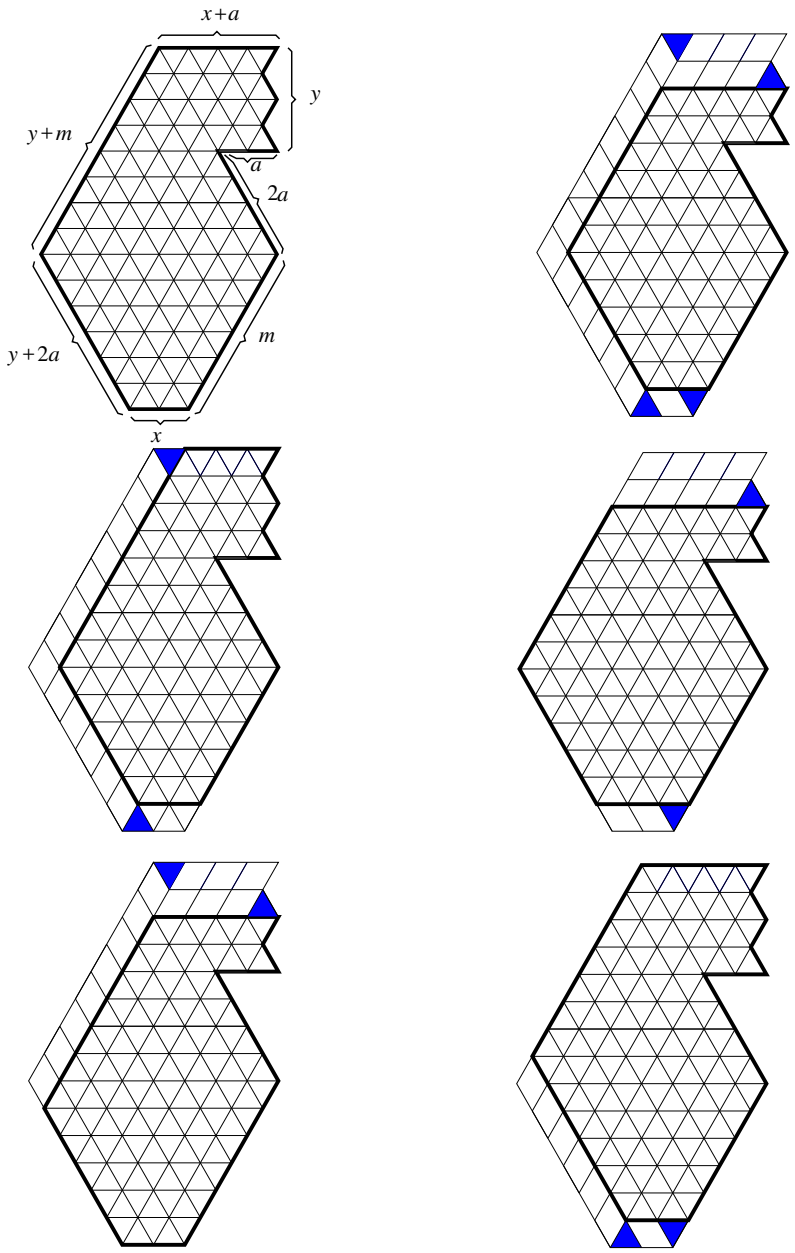

Figure 6: The recurrence for the periscope regions $\Gamma_{x,y}(m,a)$.

One readily sees that the Γ-regions can always be tiled by lozenges, so in particular we can deduce from (15) that

$$\mathrm{M}(\Gamma_{x,y}(m,a)) = \frac{1}{\mathrm{M}(\Gamma_{x,y-1}(m-1,a))}\{\mathrm{M}(\Gamma_{x-1,y}(m-1,a))\mathrm{M}(\Gamma_{x+1,y-1}(m-1,a)) + \mathrm{M}(\Gamma_{x,y-1}(m,a))\mathrm{M}(\Gamma_{x,y}(m-1,a))\}, \qquad (12)$$

for all $x, y, m \geqslant 1$.

We prove (14) by induction on $x+y+m$. Suppose that (14) holds for all non-negative integers x, y, m, a with $x + y + m < l$, and let $x, y, m \geqslant 1$ and $a \geqslant 0$ be integers with

$x + y + m = l$. Express $\mathrm{M}(\Gamma_{x,y}(m, a))$ as the expression on the right hand side of (12). By the induction hypothesis, the five quantities on the right hand side of (12) are given by formula (14). One readily checks that the resulting formula for $\mathrm{M}(\Gamma_{x,y}(m, a))$ agrees with the one given by (14). This proves the induction step.

The base cases are $x = 0$, $y = 0$, and $m = 0$. As illustrated in Figure 7, the first and third of these reduce, after removing forced lozenges, to enumerating tilings of special cases of the regions $H_s(a, b, c)$ described at the end of Section 2. For $x = 0$, the resulting formula visibly agrees with the special case $x = 0$ of (14); a straightforward calculation checks this also for $m = 0$. For $y = 0$, the region $\Gamma_{x,y}(m, a)$ becomes the hexagon of side-lengths x, $2a$, m, x, $2a$, m (in cyclic order), and one readily verifies that (14) follows from MacMahon's original enumeration [18] of boxed plane partitions (which are well-known to be in one-to-one correspondence with lozenge tilings of centrally symmetric hexagons on the triangular lattice; see e.g. [13]). This concludes our proof. □

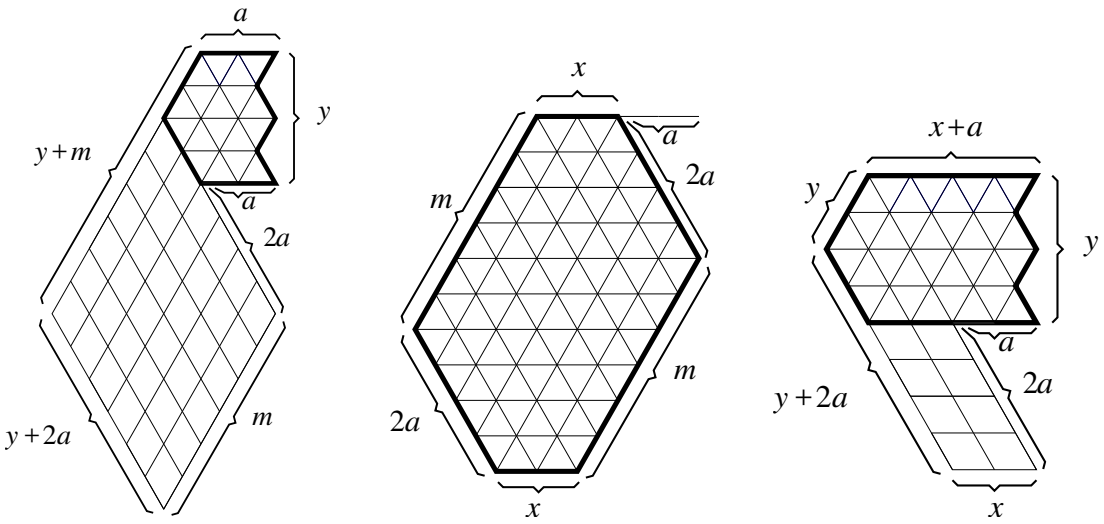

Figure 7: The base cases $x = 0$ (left), $y = 0$ (center) and $m = 0$ (right) for the regions $\Gamma_{x,y}(m, a)$.

The enumeration of tilings of the periscope regions $\Gamma'_{x,y}(m, a)$ is proved by a completely analogous inductive argument, with the only difference that equation (2) is used for the base case instead of (1). We obtain the following result.

Theorem 8. *For any non-negative integers x, y, m and a, the number of lozenge tilings of the periscope region $\Gamma'_{x,y}(m, a)$ is given by*

$$\mathrm{M}(\Gamma'_{x,y}(m, a)) = 2^y P'(y, y, a) P'(y + 2a, y + 2a + m, x) \tag{13}$$

$$\times \prod_{i=1}^{a} \frac{\left(\frac{m}{2} + i\right)_{y+2a-2i+1} \left(\frac{m}{2} + i - \frac{1}{2}\right)_{y+2a-2i+2}}{\left(x + \frac{m}{2} + i\right)_{y+2a-2i+1} \left(x + \frac{m}{2} + i - \frac{1}{2}\right)_{y+2a-2i+2}}, \tag{14}$$

where $P'(a, b, c)$ is given by (2).

4 Sigma regions Σ and Σ′

Define the sigma region $\Sigma_{x,y,k}(a,m)$ to be $R_{x,y,k}(m,a,0)$, the $b=0$ specialization of the region $R_{x,y,k}(m,a,b)$ described in Section 2. Similarly, let $\Sigma'_{x,y,k}(a,m)$ be $R'_{x,y,k}(m,a,0)$, the $b=0$ specialization of the region $R'_{x,y,k}(m,a,b)$. In this section we enumerate the tilings of these regions. They will serve as base cases for the inductive proofs of Theorems 1 and 2, which we present in the next section.

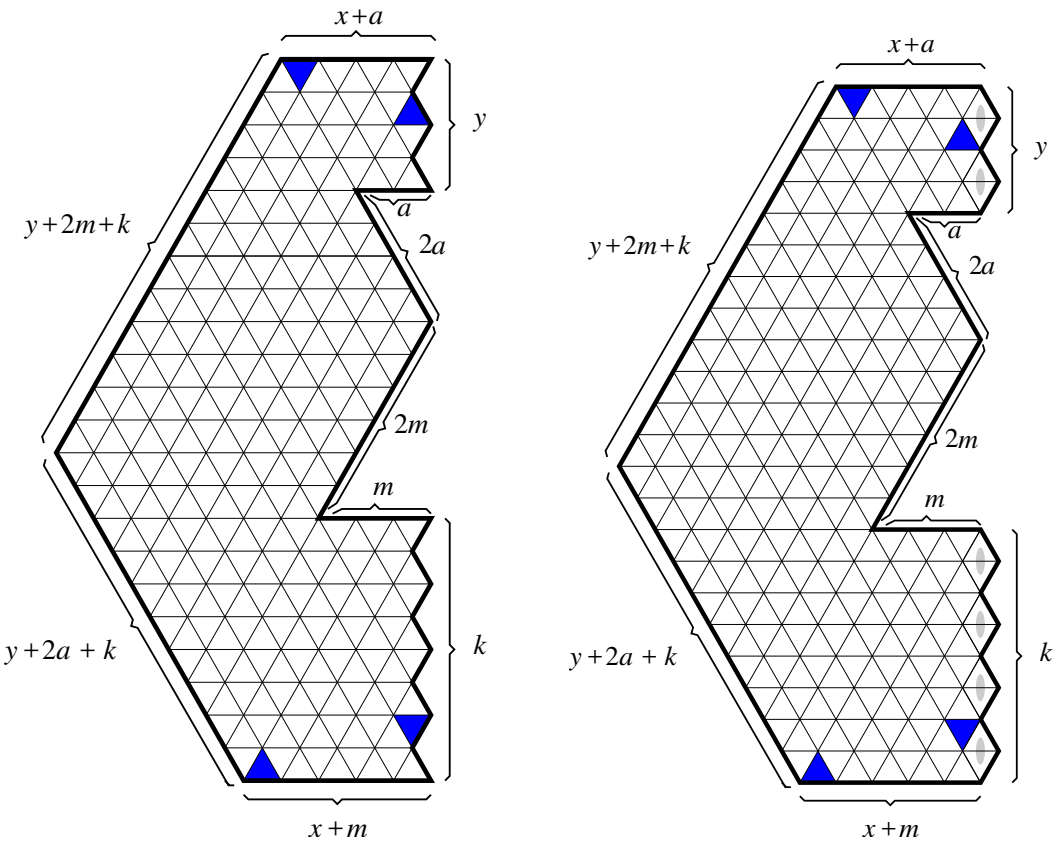

Figure 8: Applying Kuo condensation for the sigma regions.

Theorem 9. *For any non-negative integers x, y, k, m and a, the number of lozenge tilings of the sigma region $\Sigma_{x,y,k}(m,a)$ is given by*

$$\begin{aligned}\mathrm{M}(\Sigma_{x,y,k}(m,a)) &= P(k-1,k-1,m)P(y-1,y-1,a)\\ &\times \frac{P(y+2a+k-1,y+2a+k-1,x+m)}{P(y+2a+k-1,y+2a+k-1,m)}\\ &\times \prod_{i=1}^{m}\frac{(x+m-i+1)_{y+2a}(x+m+i+k)_{y+2a}}{(m-i+1)_{y+2a}(m+i+k)_{y+2a}}\\ &\times \prod_{i=1}^{a}\frac{(m+i+k)_{y+2a-k-2i+1}\left(m+i+\frac{1}{2}\right)_{y+2a+k-2i}}{(x+m+i+k)_{y+2a-k-2i+1}\left(x+m+i+\frac{1}{2}\right)_{y+2a+k-2i}}\end{aligned} \tag{15}$$

where $P(a,b,c)$ is given by (1) *when all its arguments are non-negative, and is equal to* 1 *otherwise.*

Proof. By Kuo condensation with monomers picked as in the picture on the left in Figure 8, we get (see Figure 9)

$$\begin{aligned}\mathrm{M}(\Sigma_{x,y,k}(m,a))\mathrm{M}(\Sigma_{x,y-1,k-1}(m,a)) = \\ \mathrm{M}(\Sigma_{x-1,y,k}(m,a))\mathrm{M}(\Sigma_{x+1,y-1,k-1}(m,a)) \\ + \mathrm{M}(\Sigma_{x,y-1,k}(m,a))\mathrm{M}(\Sigma_{x,y,k-1}(m,a)). \qquad (16)\end{aligned}$$

We proceed by induction on $x+y+k$. Suppose $x,y,k \geqslant 1$ (so that all the regions involved in (16) are defined), and assume that (15) holds for all the Σ-regions whose x-, y- and k-parameters add up to strictly less than $x+y+k$. By (16), $\mathrm{M}(\Sigma_{x,y,k}(m,a))$ is expressed in terms of tiling counts of Σ-regions whose sums of their x-, y- and k-parameters are strictly less than $x+y+k$, the latter being — by the induction hypothesis — given by formula (15). It is routine to verify that the resulting formula for $\mathrm{M}(\Sigma_{x,y,k}(m,a))$ agrees with the one provided by (15). This proves the induction step.

There are three base cases: $x=0$, $y=0$ and $k=0$. (There are two different sources for base cases: since (16) relates $\mathrm{M}(\Sigma_{x,y,k}(m,a))$ to Σ-regions with $(x+y+k)$-sum one or two units less, we have the base cases $x+y+k=0$ and $x+y+k=1$; in addition we have the three base cases $x=0$, $y=0$ and $k=0$, due to the fact that when any of these holds, the regions involved in (16) are not all defined. Clearly, the latter three cases cover also the former two.)

When $x=0$, the Σ-region looks as pictured in Figure 10. It is easy to see that the two half-hexagons cut out by the indicated thick dashed lines must be internally tiled in every tiling of such a region (indeed, if there were for instance a tiling of the region containing a lozenge that straddles the bottom dashed line, then starting from its bottom edge there would be a path of lozenges in this tiling that ends on a unit segment of the base; but then the m paths of lozenges starting downward from the unit segments of the inner segment of length m on the right boundary would not have enough room to end on the unit segments of the base, a contradiction). Since the tiling is obviously forced on the remaining parallelogram, it follows by (3) that

$$\mathrm{M}(\Sigma_{0,y,k}(m,a)) = P(k-1,k-1,m)P(y-1,y-1,a),$$

which is readily seen (cf. (1)) to agree with the $x=0$ specialization of the right hand side of (15). On the other hand, if $y=0$ or $k=0$, the Σ-region clearly reduces to a periscope region, and its enumeration follows therefore from Theorem 7. It is straightforward to verify that the resulting formulas agree with the $y=0$ and $k=0$ specializations of the right hand side of (15), respectively. This completes the proof. □

The same arguments prove the following result.

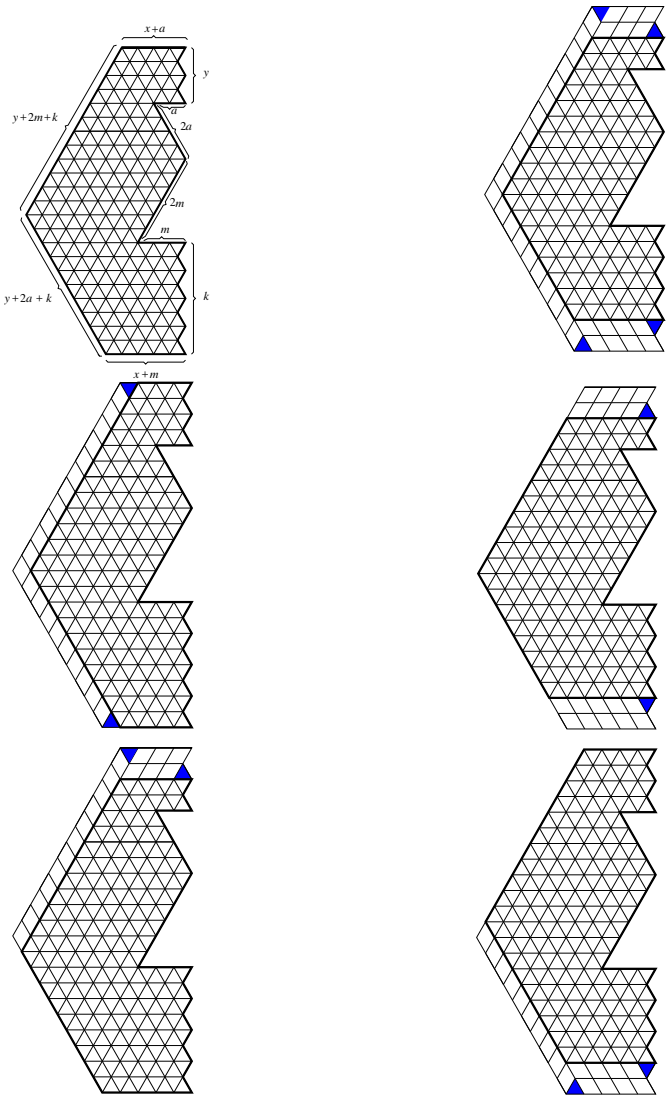

Figure 9: The recurrence for the sigma regions $\Sigma_{x,y,k}(m,a)$.

Theorem 10. *For any non-negative integers x, y, k, m and a, the number of lozenge tilings of the sigma region $\Sigma_{x,y,k}(m,a)$ is given by*

$$\begin{aligned}\mathrm{M}(R'_{x,y,k}(m,a,b)) &= 2^{y+2a}P'(k,k,m)P'(y,y,a)\frac{P'(y+2a+k,y+2a+k,x+m)}{P'(y+2a+k,y+2a+k,m)}\\ &\times\prod_{i=1}^{m}\frac{(x+m-i+1)_{y+2a}(x+m+i+k)_{y+2a}}{(m-i+1)_{y+2a}(m+i+k)_{y+2a}}\\ &\times\prod_{i=1}^{a}\frac{(m+i+k)_{y+2a-k-2i+1}\left(m+i-\frac{1}{2}\right)_{y+2a+k-2i+2}}{(x+m+i+k)_{y+2a-k-2i+1}\left(x+m+i-\frac{1}{2}\right)_{y+2a+k-2i+2}},\end{aligned} \tag{17}$$

where $P'(a,b,c)$ is given by (2).

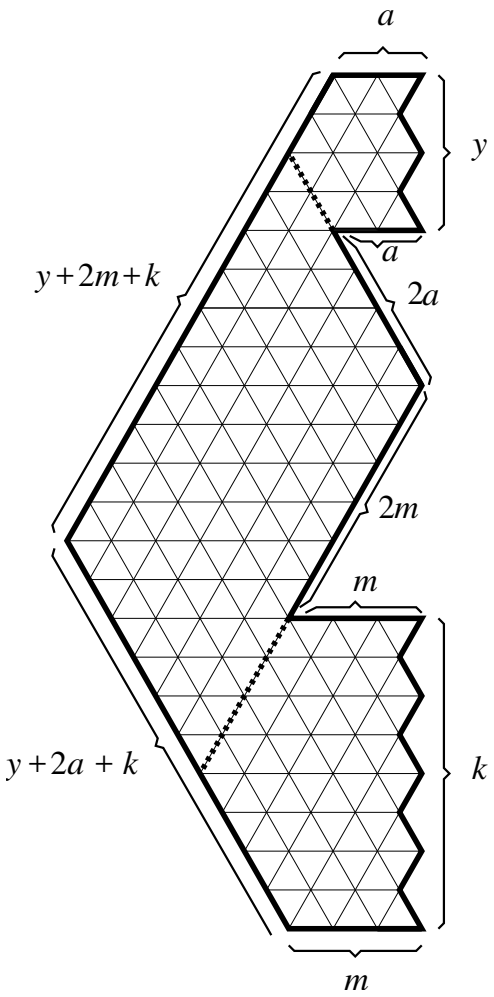

Figure 10: The base case $x = 0$ for the sigma regions $\Sigma_{x,y,k}(m, a)$.

5 Proofs of Theorems 2.1–2.2

We prove our results by induction, relying on Kuo's graphical condensation method [15] at the induction step, and on the results of Sections 3 and 4 for the base cases.

We present the details for the proof of Theorem 1. The proof of Theorem 2 is obtained by the same arguments, with exactly the same arguments at the induction step, and minimal modifications for the base cases.

Consider the region obtained from $R_{x,y,k}(m, a, b)$ by reducing by one unit the side-length of the lobe of side b, as illustrated in the picture on the left in Figure 11, and choose the four monomers in Kuo's graphical condensation (the version of Theorem 6) as indicated in that figure.

Each of the six regions involved in the resulting recurrence is readily seen to become, after conveniently removing some of the forced lozenges (operation which preserves the number of lozenge tilings), one of our regions of type R. More precisely, as can be seen

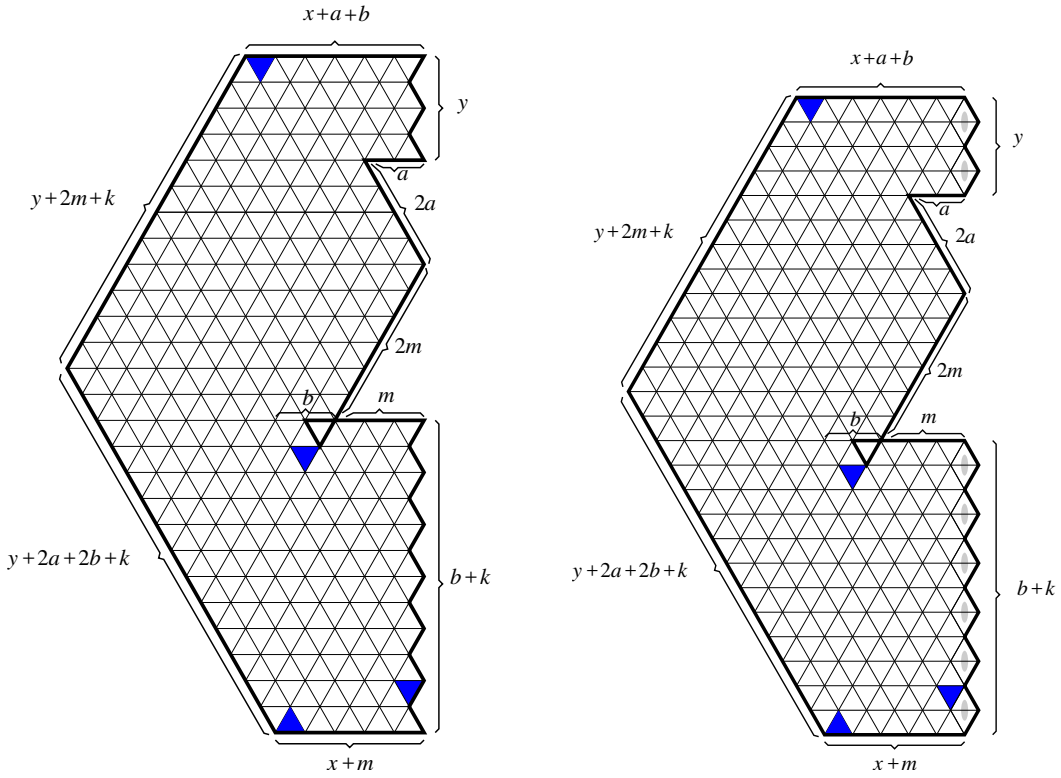

Figure 11: Choosing the monomers in the regions $R_{x,y,k}(m,a,b)$ and $R'_{x,y,k}(m,a,b)$.

from Figure 12, we obtain the recurrence

$$\mathrm{M}(R_{x,y,k}(m,a,b))\mathrm{M}(R_{x,y,k}(m,a,b-1)) = \tag{18}$$
$$\mathrm{M}(R_{x,y,k+1}(m,a,b-1))\mathrm{M}(R_{x,y,k-1}(m,a,b)) \tag{19}$$
$$+\,\mathrm{M}(R_{x+1,y,k}(m,a,b-1))\mathrm{M}(R_{x-1,y,k}(m,a,b)). \tag{20}$$

We claim that this recurrence is valid for all integers $x,k,b \geqslant 1$ and $y,m,a \geqslant 0$ (clearly necessary conditions for the involved regions to be defined).

Indeed, the indicated choices for the monomers (see the picture on the left in Figure 11) are possible (in other words, there is room for the indicated monomers) provided $x+m \geqslant 1$, $x+a+b \geqslant 1$, $b \geqslant 1$ and $b+k \geqslant 1$. In turn, all these inequalities clearly hold if $x,k,b \geqslant 1$. Furthermore, the pattern of forced tiles indicated in Figure 12 is valid provided $x,k,b \geqslant 1$. Finally, for instance the fact that the lobe of side length b fits inside the region indicated by the thick contour in the center right picture in Figure 12 does not need to be checked, being guaranteed by the very fact that the latter is a region of type R (namely, $R_{x,y,k-1}(m,a,b)$; see the observation in the fourth paragraph of Section 2). This completes the proof of (20) for all $y,m,a \geqslant 0$ and $x,k,b \geqslant 1$. The base cases of our induction will be $x=0$, $k=0$ and $b=0$.

Proof of Theorem 1. Use (20) to express $\mathrm{M}(R_{x,y,k}(m,a,b))$ in terms of the other five quantities in that equation. We want to regard the resulting expression as a recurrence for $\mathrm{M}(R_{x,y,k}(m,a,b))$. Note that the sum of the x-, k- and b-parameters — the most natural quantity to consider — is not strictly less than $x+k+b$ for all five R-regions

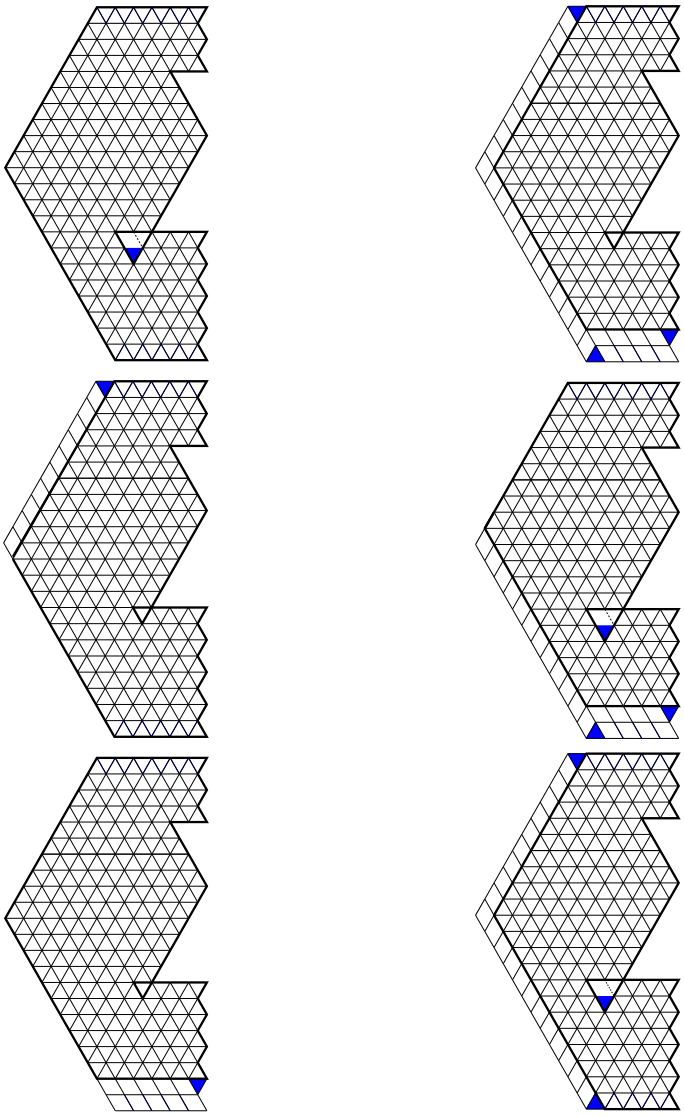

Figure 12: The recurrence for the regions $R_{x,y,k}(m,a,b)$.

in (20) other than $R_{x,y,k}(m,a,b)$. However, for each of these five regions, adding the x-, k- and *twice* the b-parameter results in a quantity that is either 1 or 2 units less than $x+k+2b$. We proceed therefore by induction on $x+k+2b$.

Let $x,k,b \geqslant 1$, and assume that (6) holds for all R-regions in which the sum between the x-, y- and twice the b-parameter is strictly less than $x+k+2b$. Then (20) yields, by the induction hypothesis, an explicit expression for $\mathrm{M}(R_{x,y,k}(m,a,b))$ obtained by applying formula (6) to the other five quantities in (20). A straightforward calculation verifies that this expression agrees with the right hand side of (6). This proves the induction step.

The base cases of the induction are $x=0$, $k=0$, and $b=0$. For $b=0$, the region $R_{x,y,k}(m,a,b)$ becomes the sigma region $\Sigma_{x,y,k}(m,a)$, and its tiling count follows by Theorem 9. The resulting expression visibly agrees with the $b=0$ specialization of the right hand side of (6).

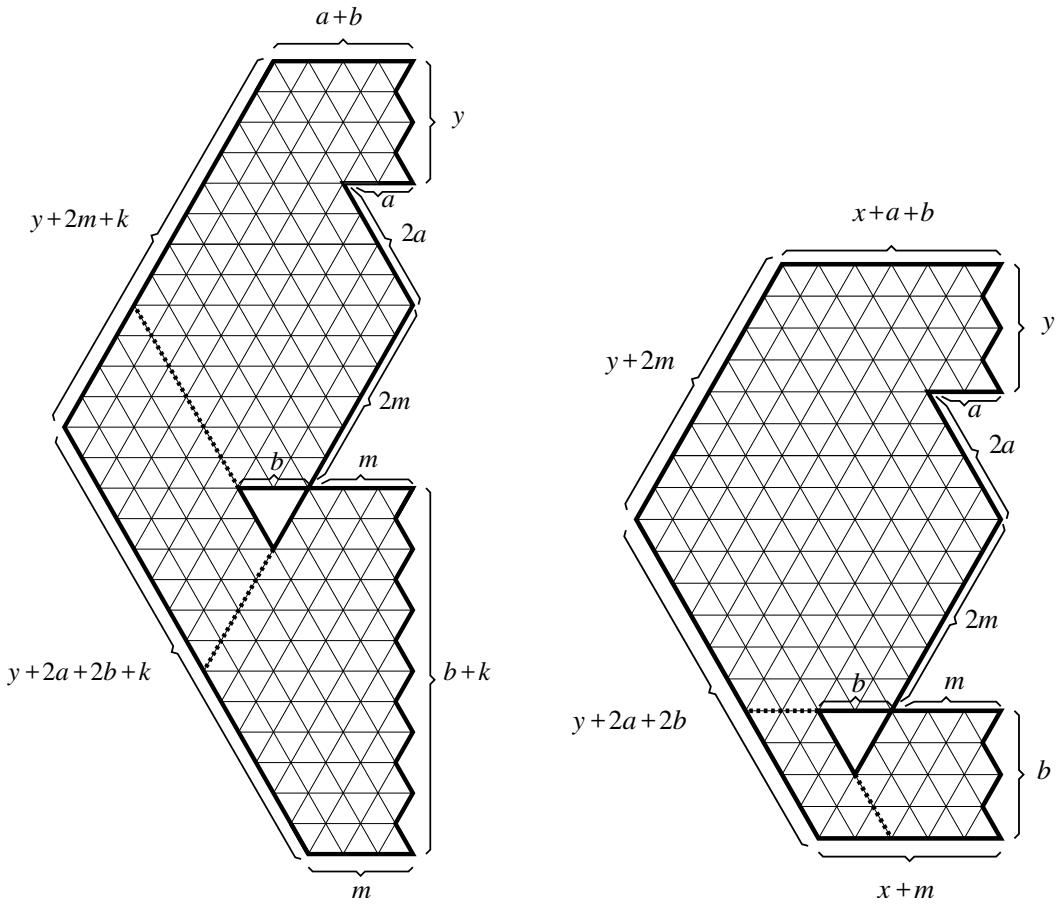

Figure 13: The base cases $x = 0$ (left) and $k = 0$ (right) for the regions $R_{x,y,k}(m, a, b)$.

For $x = 0$, the R-region looks as illustrated in the picture on the left in Figure 13. Using the same argument as in the proof of Theorem 9, one readily sees that the half-hexagon cut out by the bottom thick dashed line in the picture on the left in Figure 13 must be internally tiled. This in turn forces the indicated parallelogram to be tiled internally. It follows that the periscope region delimited by the top thick dashed line is also internally tiled, and therefore

$$\mathrm{M}(R_{0,y,k}(m, a, b)) = P(b + k - 1, b + k - 1, m)\mathrm{M}(\Gamma_{b,y+2a}(2m, a)). \tag{21}$$

One readily checks that the formula resulting from (21) using (1) and Theorem 7 agrees with the $x = 0$ specialization of the right hand side of (6). The base case $k = 0$ follows analogously, using that, as seen from the picture on the right in Figure 13,

$$\mathrm{M}(R_{x,y,0}(m, a, b)) = P(b - 1, b - 1, m)\mathrm{M}(\Gamma_{b+x,y+2a}(2m, a)). \tag{22}$$

This completes the proof. □

The proof of Theorem 2 is perfectly analogous. One applies Kuo condensation as indicated in the picture on the right in Figure 11 (note that the choice of the monomers is precisely the same as above). The previous proof of the induction step carries over

with no change. The only difference is that at the base cases we now use the counterparts Theorem 10, Theorem 8 and (4) of Theorem 9, Theorem 7 and (3), respectively.

6 The core position that maximizes the number of tilings

Since the shamrock hole can glide up and down along the vertical symmetry axis, a natural question is for which position is the number of tilings maximum.

We can gain some intuition about this by recalling the electrostatic interpretation of random tilings with gaps worked out in our previous work [5][6][7][9][10]: If gaps are viewed as electrical charges of magnitude given by the difference between the number of up- and down-pointing unit triangles in them, then for large separations between the gaps, the probability of any position of the gaps is proportional to the exponential of the negative 2D Coulomb energy of the system.

We only have one gap in our current situation (the central shamrock), of charge $2m-2a-2b$, but the set-up is such that this gap feels the interaction with the boundary of the dimer system — more precisely, since it is allowed to glide along the symmetry axis, the interaction with the top and bottom sides of the outer hexagon. Since both these boundaries are constrained lattice lines, for $2m-2a-2b \neq 0$ we expect (see [10] and [11]) an exponentially strong interaction with the boundary — overwhelming attraction to the bottom side for $2m-2a-2b > 0$, and overwhelming attraction to the top side for $2m-2a-2b < 0$.

Therefore, the interesting case to consider is that when the central shamrock has charge zero, i.e. $2m-2a-2b = 0$.

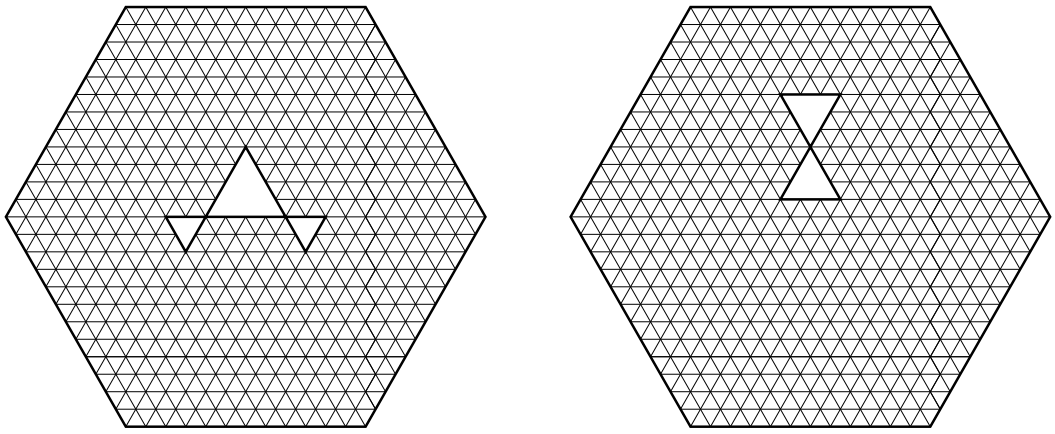

Figure 14: The case $a = 0$ (left) and the case $b = 0$ (right).

If $a = 0$, then the axial shamrock looks as pictured on the left in Figure 14. Since the top lobe has then positive charge (as the a-lobe disappears) and the two bottom lobes have negative charge, we expect (and this is confirmed by numerical examples) that the central shamrock will be repelled both by the top and by the bottom sides of the outer hexagon, and thus that the position with maximum number of tilings will be somewhere in the interior. At the other extreme, when $a = m$ and $b = 0$, the axial shamrock looks as

pictured on the right in Figure 14, and by the same heuristics we expect (and this is again confirmed by numerical examples) that both the top and the bottom side will attract the central shamrock, and that the maximum will occur when the central shamrock touches one of these sides. Furthermore, for $a << b$ we expect the former kind of behavior, while for $a >> b$ the latter. The interesting question is to describe the point at which one behavior changes into the other.

Numerical examples suggest that there exists a critical ratio $r = 1.5\ldots$ so that for large enough outer hexagons, if a and b are fixed[4] and $b/a < r$ then the first kind of behavior occurs, while if $b/a > r$ then the second kind holds. This could be verified using our explicit formula for $\mathrm{M}(AS_{x,y,k}(m,a,b))$ given in Corollary 3, but the calculations are somewhat complicated and we have not carried them out.

An interesting variation is to consider the same question, but to scale the central shamrock together with the outer boundary.

7 Concluding remarks

Upon looking at the region $R_{x,y,k}(m,a,b)$ on the left in Figure 2 (or even directly at Figure 1) one may notice the following lack of symmetry: There is a triangular lobe attached to the lower corner of the Σ-shaped portion of the eastern boundary, but no lobe attached to the upper corner. Surely, one might say, the more general region obtained including one lobe there as well in order to restore this symmetry (and the similar extension of the region $R'_{x,y,k}(m,a,b)$) should also have its number of lozenge tilings given by a simple product formula. This would imply, by the factorization theorem of [3], that tilings of regions of the type illustrated in Figure 15 are also enumerated by such a product formula.

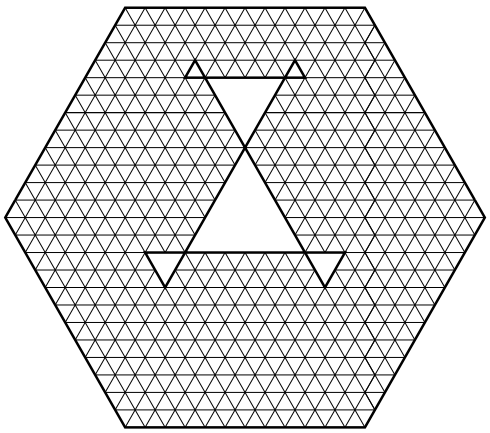

Figure 15: A possible generalization of axial shamrocks.

However, this doesn't seem to be the case. Numerical examples show that relatively large primes occur in the factorization of the number of tilings of such regions, which does not happen in a product formula where all factors are linear in the parameters

[4] Since we are discussing the case of the neutral central shamrock, fixing a and b fixes m as well, as $m = a + b$.

(this happens even in the most symmetric case, when the outer hexagon is regular, and the removed structure is symmetric about the center). It would be interesting to find a formula for the number of tilings of these more general regions.

References

[1] G. E. Andrews. Plane partitions (III): The weak Macdonald conjecture. *Invent. Math.*, 53:193–225, 1979.

[2] D. M. Bressoud. Proofs and confirmations — The story of the alternating sign matrix conjecture. Cambridge University Press, Cambridge, 2009.

[3] M. Ciucu. Enumeration of perfect matchings in graphs with reflective symmetry. *J. Combin. Theory Ser. A*, 77:67–97, 1997.

[4] M. Ciucu and C. Krattenthaler. Enumeration of lozenge tilings of hexagons with cut off corners. *J. Combin. Theory Ser. A*, 100:201–231, 2002.

[5] M. Ciucu. A random tiling model for two dimensional electrostatics. *Mem. Amer. Math. Soc.* , 178:1–106, no. 839, 2005.

[6] M. Ciucu. The scaling limit of the correlation of holes on the triangular lattice with periodic boundary conditions. *Mem. Amer. Math. Soc.*, 199:1–100, no. 935, 2009.

[7] M. Ciucu. Dimer packings with gaps and electrostatics. *Proc. Nat. Acad. Sci. USA*, 105:2766–2772, no. 8, 2008.

[8] M. Ciucu and C. Krattenthaler. A dual of MacMahon's theorem on plane partitions. *Proc. Natl. Acad. Sci. USA*, 110:4518–4523, 2013.

[9] M. Ciucu. The interaction of collinear gaps of arbitrary charge in a two dimensional dimer system. *Comm. Math. Phys.*, 330:1115–1153, 2014.

[10] M. Ciucu. Macroscopically separated gaps in dimer coverings of Aztec rectangles. *Comm. Math. Phys.*, 344:223–274, 2016.

[11] M. Ciucu. Lozenge tilings with gaps in a 90° wedge domain with mixed boundary conditions. *Comm. Math. Phys.*, 334:507–532, 2015.

[12] M. Ciucu. Symmetries of shamrocks, Part I. *J. Combin. Theory Ser. A*, 155:376–397, 2018.

[13] G. David and C. Tomei. The problem of the calissons. *Amer. Math. Monthly*, 96:429–431, 1989.

[14] C. Koutschan, M. Kauers and D. Zeilberger. A proof of George Andrews' and David Robbins' q-TSPP-conjecture. *Proc. Natl. Acad. Sci. USA*, 108:2196–2199, 2011.

[15] E. H. Kuo. Applications of graphical condensation for enumerating matchings and tilings. *Theoret. Comput. Sci.*, 319:29–57, 2004.

[16] E. H. Kuo. Graphical condensation generalizations involving Pfaffians and determinants. arXiv:math/0605154, 2006.

[17] G. Kuperberg. Symmetries of plane partitions and the permanent-determinant method. *J. Combin. Theory Ser. A*, 68:115–151, 1994.

[18] P. A. MacMahon. Combinatory Analysis, vols. 1–,. Cambridge, 1916, reprinted by Chelsea, New York, 1960..

[19] R. A. Proctor. Odd symplectic groups. *Invent. Math.*, 92:307–332, 1988.

[20] R. P. Stanley. Symmetries of plane partitions. *J. Comb. Theory Ser. A*, 43:103–113, 1986.

[21] J. R. Stembridge. The enumeration of totally symmetric plane partitions. *Adv. in Math.*, 111:227–243, 1995.